Bulletin of Engineering Geology and the Environment (2021) 80:7029–7049
https://doi.org/10.1007/s10064-021-02363-7

ORIGINAL PAPER

Response characteristics and mechanism of the strength and energy of schist to the schistosity orientation and water

Xiaomeng Yin[1,2] · Xia Zhang[2] · Yuju Lei[3] · Lunan Wang[4]

Received: 11 December 2020 / Accepted: 4 July 2021 / Published online: 15 July 2021

Abstract

In this study, uniaxial compression testing was carried out to investigate the response of quartz mica schist to water in terms of strength and energy anisotropy. The micromechanism and water action mechanism of the anisotropic properties of the schist were further discussed based on microscopic observations of the rock fabric and analysis of the mineral composition of the solid precipitant after immersion. Mechanical tests reveal that both the failure strength and crack initiation strength of dry schist change in a U shape with the schistose angle; moreover, the strength anisotropy of schist generally increases with increasing immersion time. The specimen with $\alpha = 30°$ has the minimum energies, while that with $\alpha = 90°$ exhibits the maximum total and elastic energies. The total and elastic energies of dry specimens decrease significantly after saturation, but the influence degree of water on the energy of schist differs with the schistosity orientation. The energy response of specimens with $\alpha = 30°$ and 0° to water is more sensitive than that with $\alpha = 90°$. The internal energy allocation of schist was found to be associated with the schistosity orientation and immersion time. Based on the analysis of microcrack propagation and macro-failure, it is concluded that the fabric of schist plays an essential controlling role in the strength and energy anisotropy. The response of anisotropy to water is closely dependent on the lubrication and disintegration of flaky minerals and the hydraulic action on the tips of voids in response to external compression.

Keywords Schist · Anisotropy · Crack initiation strength · Energy · Water action mechanism

Introduction

Among the three generic categories of rocks, many sedimentary and metamorphic rocks exhibit significant anisotropy due to the development of bedding planes or schistosity. As a commonly notable property of rocks with weak planes, anisotropy not only has important research significance in seismic wave dynamic characteristics and seismic response in the geoscience field but also receives extensive attention in the geotechnical engineering field. Anisotropy is a nonnegligible factor in the designs of ground and foundation, slope, underground engineering and stability analyses of geological bodies. Since the 1960s, the anisotropy of rock and soil has been a popular topic in geotechnical engineering.

In view of the outstanding problems in different projects, geotechnical engineers place various emphases on the study of rock (or rock mass) anisotropy, including that of the physical, hydraulic and mechanical properties. The mechanical anisotropy of rocks with weak planes is a topical issue that has been discussed continuously because the elastic properties and the compressive or tensile strengths of rock are usually considered to be crucial factors in the design of various geotechnical engineering projects (Peng and Johnson 1970). Especially in the aspect of the strength anisotropy of rocks, abundant achievements have been made (Cho et al. 2012; Donath 1964; Gholami and Rasouli 2014; Hoek 1964; Khanlari et al. 2015; McLamore and Gray 1967; Nasseri et al. 2003; Singh et al. 1989). The results show that the compressive strength often changes in a U shape, shoulder shape or wave shape with increasing angle β between the

✉ Yuju Lei
leiyuju0903@163.com

1 College of Intelligent Construction, Wuchang University of Technology, Wuhan 430223, China

2 College of Architecture and Civil Engineering, Xinyang Normal University, Xinyang 464000, China

3 School of Education, Hubei University of Art and Science, Xiangyang 441053, China

4 School of Civil Engineering, Liaoning Petrochemical University, Fushun 113001, China

loading direction and weak planes. The maximum compressive strength corresponds to $\beta = 0°$ or 90°. The minimum value is in the range of $\beta = 20$ to 50°, theoretically located at $\beta = 45° - \varphi/2$ (φ is the internal friction angle of the weak planes) (Nasseri et al. 2003). Macroscopically, strength anisotropy is closely related to the type of rock itself, the development degree of weak planes etc. and is affected by the external stress environment. Reviewing these studies, we find that most researchers mainly focus on the ultimate compressive strength.

A large number of weakly weathered rocks exhibit brittle failure under compression. Stress concentrations are prone to occur at the tips of existing defects in rock subjected to compression. Then, new cracks are induced, followed by crack propagation and the coalescence of large numbers of cracks, which eventually leads to the formation of a through failure surface and causes the rock to lose its bearing capacity. Thus, the brittle failure of rock is essentially attributed to the gradual evolution of the crack system, characterized by progressive deformation and fracture development. In fact, the instability of a considerable proportion of geological bodies composed of rock masses is not sudden in practical engineering. Before instability, these bodies often go through the process of the local appearance and connection of fracture surfaces, which is quite common in the failure of perilous rock in high and steep slopes and the surrounding rock of underground engineering. In view of this, only focusing on the ultimate compressive strength of rock yields a limited perspective. The division of the crack evolution stages and discrimination of the critical conditions of different stages are of great significance for evaluating the stability of rock masses and engineering safety. In the mid- and late twentieth century, Brace et al. (1966), Bieniawski (1967), Martin (1997) and Eberhardt et al. (1998) divided the deformation and failure of brittle rock into several stages through experimental study. It is recognized that the failure of brittle rock begins with the initiation of new cracks, and the crack initiation strength indicates the critical stress from linear elasticity to nonlinear deformation, which is an important index of rock fracture mechanics. Subsequently, a series of studies on the indicative significance and trends of characteristic strengths along with crack evolution in rock were carried out.

According to Xie et al. (2005), the destruction of material is a state instability phenomenon driven by energy. The initiation, propagation and coalescence of cracks in rock subjected to compression are always accompanied by energy conversion between internal and external systems, which can be used to characterize continuous changes in material properties and states (Mikhalyuk and Zakharov 1997; Steffler et al. 2003; Sujatha and Kishen 2003). The characteristics of damage evolution can be studied from the view of energy, which points to the essence of rock failure. In recent years, rock mechanics researchers have carried out many studies in this field. Great efforts have been made towards describing the deformation and failure behaviour of rock masses by energy analysis, and the relevant results have been preliminarily applied to engineering practice. Previous studies on the energy conversion and dissipation of rocks mainly aimed to establish the criterion of crack propagation (Bańka et al. 2017; Griffith 1921), to quantitatively evaluate the possibility of rock bursts based on a reliable energy index (Cai et al. 2001; Goodman 1989; Kidybinski 1981; Yang et al. 2019) and to create an evaluation method of rock brittleness (Chen et al. 2020; Zhang et al. 2017).

The mechanical properties of rock are not only related to mineral composition and microstructure but also affected by its environmental conditions, especially those regarding groundwater. Water is one of the important factors in evaluating the quality of engineering rock masses and analysing their stability. The complex physical, chemical and mechanical interaction between water and rock has a significant impact on the strength and energy of rock. Previous studies show that (1) the water molecules in intergranular spaces weaken the friction factor and cohesion between particles; (2) the internal structure of rock is damaged by the dissolution effect of water on minerals with poor chemical stability; and (3) the water film of minerals with high hydrophilicity thickens, and the minerals are softened and expanded, causing uneven stress in the rock (Baud et al. 2000; Eeckhout 1976; Zhao et al. 2016). These physical and chemical actions eventually lead to changes in rock properties, such as decreases in fracture toughness and surface energy and the deterioration of resistance to deformation and failure (Haberfield and Johnston 1990; Roy et al. 2017). In addition, the mechanical action of water has an important effect on the distributions of stress and energy in rock, which changes the threshold of crack initiation and plays an important role in the process of crack evolution. The effect of fluid pressure magnifies the stress intensity factor around a crack tip, which is conducive to inducing new cracks (Detournay et al. 1989). Based on Griffith's strain energy release criteria, Bruno and Nakagawa (1991) derived that tensile fracture in a poroelastic body is directly controlled by the effective stress. They found that the pore pressure magnitude contributes to the initiation of tensile fracture in high-porosity rocks and that pore pressure gradients play an important role in fracture propagation.

It is well acknowledged that the influence of water on rock closely depends on the time of water–rock interaction and water content. Vishal et al. (2015) and Yao et al. (2016) found that the crack initiation strength of coal rock decreases in a negative exponential form and that the damage strength decreases in a linear form with increasing water content. Guo et al. (2007) and Xia et al. (2015) found that in a state without confining pressure, the

compressive strength of saturated rock decreases exponentially with the immersion time and finally tends to be constant. Some researchers recognize that the influence effect of water on rock is associated with the stress condition. Different from static loading, the water in rock subjected to dynamic loading hinders the generation and expansion of cracks; this involves some complex effects of water, such as the meniscus effect, visibility effect and enhancement effect on rock inertia (Rossi 1991; Wang et al. 2009; Zhang and Zhao 2013). Compared with that under low confining pressure, rock under high confining pressure experiences a more obvious immersion time effect (Guo et al. 2007). It is thus clear that the effect and mechanism of water on rocks are quite complex. Although abundant achievements have been made on water–rock interactions, these issues still need continuous attention.

At present, the study on the crack initiation strength and energy conversion under compression is mainly focused on homogeneous rocks, less on rocks with weak planes, and few achievements involve the influence of water on the strength and energy of anisotropic rocks. In this study, the fabric of a quartz mica schist with obvious schistosity was explored by microtests. Then, a uniaxial compression test was performed on cylindrical specimens with various orientation angles. The response trends of the crack initiation strength and energy conversion to the loading direction and water were investigated, and the physico-mechanical mechanism was further discussed. This study can provide theoretical guidance for the stability analysis and prediction of rock slopes and surrounding rock, as well as the design and construction of underground engineering.

Geology of the site and physical properties of the rock sample

The samples were obtained from the large-span Tongsheng tunnel, which is distributed on the expressway connecting Shiyan City and Fang County of Hubei Province in China (Fig. 1). The project area is located on the northern margin of the Yangtze platform and in the range of the South Qinling orogenic belt. It has experienced multiple stages of deformation, metamorphism and magmatism. The landform of middle mountains suffering from tectonic denudation is characterized by large undulation and strong cutting on the terrain.

The strata in the area belong to the Proterozoic Wudang Group (Pt_2wd), which is mainly distributed in Shiyan City, from Yunxi County in the north to Fang County in the south. The protolithic rocks of the Wudang Group are mainly composed of acidic volcanic rocks, basic volcanic rocks and sedimentary rocks (dual-mode volcanic rock-sedimentary rock combination (Zhou et al. 1996); Fig. 1b). A set of metamorphic rock series including meta-granite, meta-sandstone, schist, marble and quartzite form the Wudang Group (Liu et al. 1992). Although the lithology of the Wudang Group schist, as the main rock exposed in the project area, is complex and diverse, it is mainly composed of quartz mica schist with typical lepidoblastic texture and fairly developed schistosity. In some parts seriously affected by weathering, the quality of the surrounding rock of the tunnel greatly deteriorates through argillization when the rock encounters groundwater. The samples in this study were taken from tunnel sections with weak weathering and good integrity surrounding rock. The notable anisotropy of the schistose surrounding

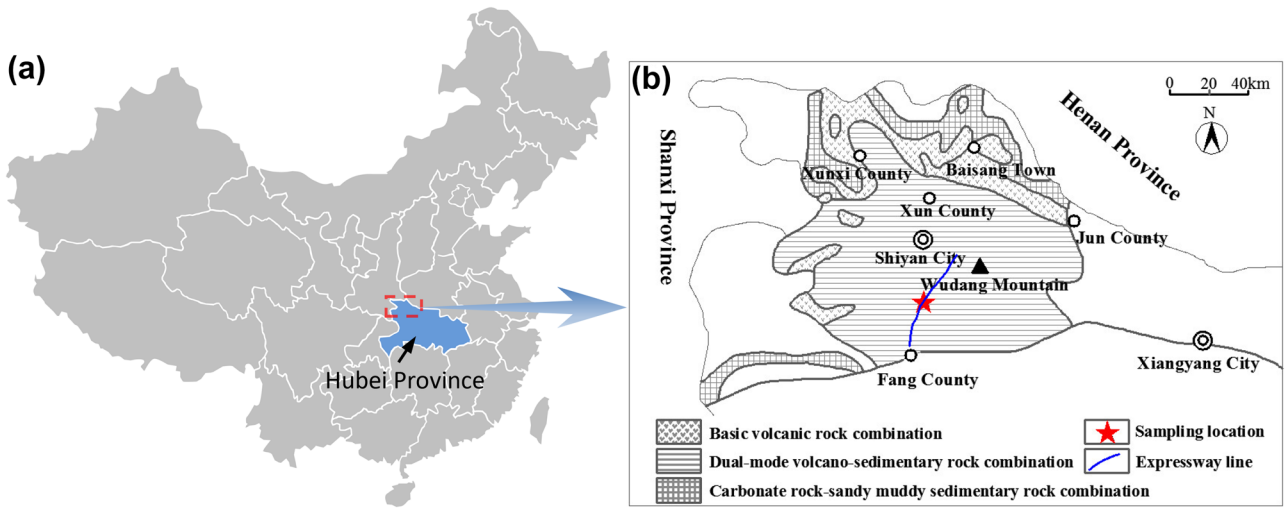

Fig. 1 Sampling location and distribution of metamorphic strata: (**a**) location of sampling points in China; (**b**) distribution of protolithic rock combination in metamorphic belt of Northwest Hubei Province

rock in these parts has received much attention by the design department due to its adverse impact on engineering support. The schist sample is shown in Fig. 2.

A physical property test was carried out to obtain the relevant parameters of the samples in accordance with "Standard for tests method of engineering rock masses" (GB/T 50,266–2013, 2013). The average values are as follows: natural density, 2.675 g/cm^3; saturated density, 2.684 g/cm^3; saturated water content, 0.86%; and porosity, 2.30%. Here, the density was measured by the volume product method, the saturated water content was obtained by the vacuum pumping method and the porosity was calculated by $n=(m_w-m_d)/(\rho_w v)$, where m_w and m_d represent the saturated mass and dry mass of the sample, respectively; ρ_w is the density of water; and v is the volume of the sample.

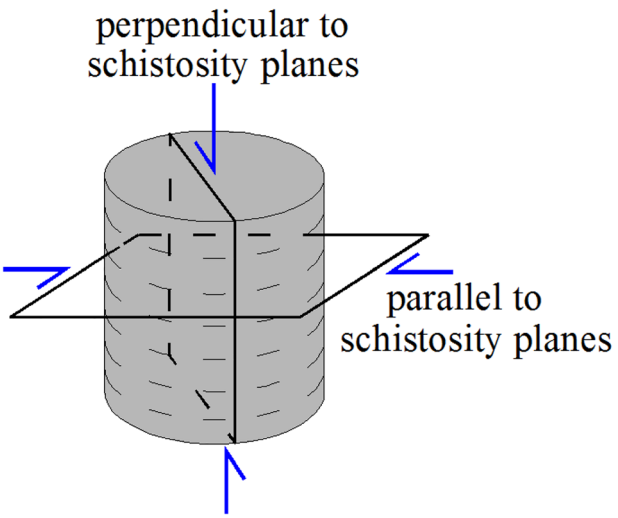

Fig. 3 Grinding direction for optical thin sections

Fabric characteristics of the rock sample

Optical thin sections with two different orientations were obtained after grinding the surface of the rock blocks perpendicular and parallel to the schistosity planes (Fig. 3). Polarizing microscopy was utilized to analyse the composition, morphology and arrangement characteristics of the minerals. The schist is mainly composed of quartz, feldspar, muscovite and calcite. In addition, a small amount of chlorite, as the weak weathering product of the rock, always appears near the muscovite minerals. The content of the mineral was determined by X-ray powder diffraction analysis. The average mineral percentages are as follows: quartz, 48%; muscovite, 27%; feldspar, 16%; calcite, 6%; and chlorite, 2%. Affected by certain temperatures and pressures, the minerals are elongated to varying degrees in the process of formation. In particular, the flaky muscovite tends to be oriented along its dominant long axis. Suffering from metamorphic differentiation, the muscovite minerals are prone to gathering into multiple weak layers nearly parallel to each other at the microlevel, thus forming macro-schistosity planes. Undulatory extinction of quartz is observed, indicating lattice dislocation in the mineral crystals caused by high in situ stress acting on the rock.

Fig. 2 Rock sample

According to the morphological characteristics, the minerals can be divided into two types of units. One is flaky minerals represented by muscovite, and the other is granular minerals mainly involving quartz, feldspar and calcite. In the directions perpendicular to (Fig. 4a) and parallel to (Fig. 4b) the schistosity planes, the minerals exhibit different arrangement characteristics. Figure 4a shows that the slender layers containing flaky muscovite intermittently "fill" between the strong zones composed of granular quartz, feldspar and calcite, forming an overall nearly interbedded structure. Figure 4b shows that quartz, feldspar and calcite particles are closely chimaeric with each other through concave and convex irregular surfaces. The heterogeneity of the schist is caused by the above arrangement of minerals, which in essence leads to the macroscopic physico-mechanical anisotropy of the rock.

The samples were cut along the direction perpendicular to the schistosity planes to make small cubic thin slices with lengths, widths and thicknesses of 2 cm, 2 cm and 0.8 cm,

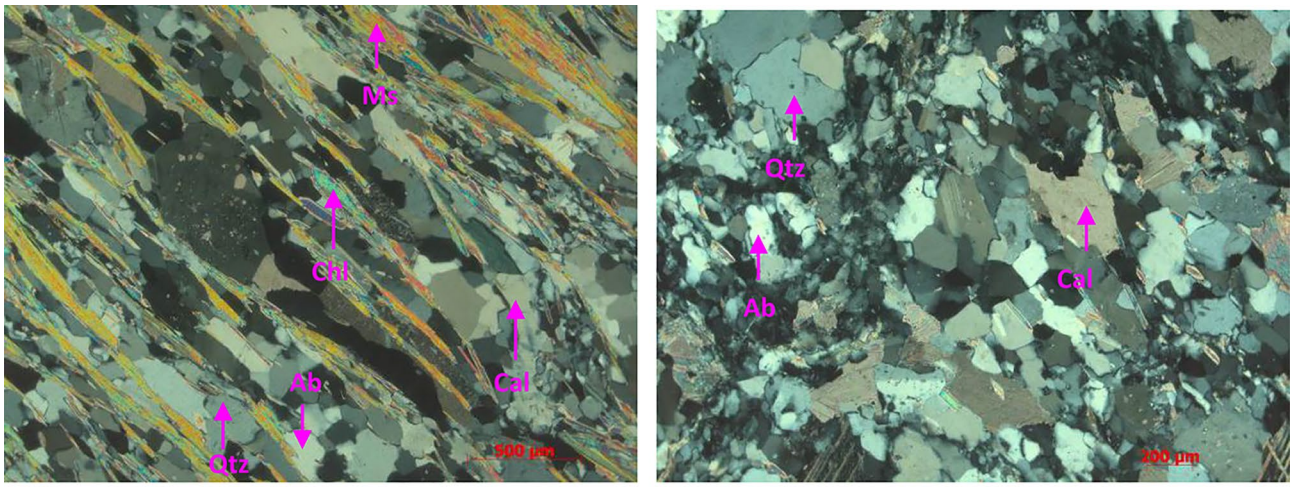

(a) Perpendicular to schistosity planes **(b)** Parallel to schistosity planes

Fig. 4 Polarizing microscope images: (**a**) perpendicular to schistosity planes; (**b**) parallel to schistosity planes. In (**a**), represents flaky muscovite (Ms)

respectively. A series of operations on the rectangular surface of 2 cm × 2 cm perpendicular to the schistosity planes, including rough grinding, fine grinding, polishing, drying and carbon coating, were carried out in turn to make optical slices. A Quanta 200 environmental scanning electron microscopy (ESEM) was used to further observe the microstructure of the schist. The greyscale image obtained with the ESEM (Fig. 5) shows that pores and microcracks with different scales exist in the schist. The large-scale microcracks, also exhibiting a certain degree of orientability and stratoid distribution, are mainly distributed along the edge of the aggregated muscovite layer, suggesting a low bonding strength at the edges of the flaky minerals. The extension direction of the pores and microcracks in other parts is irregular.

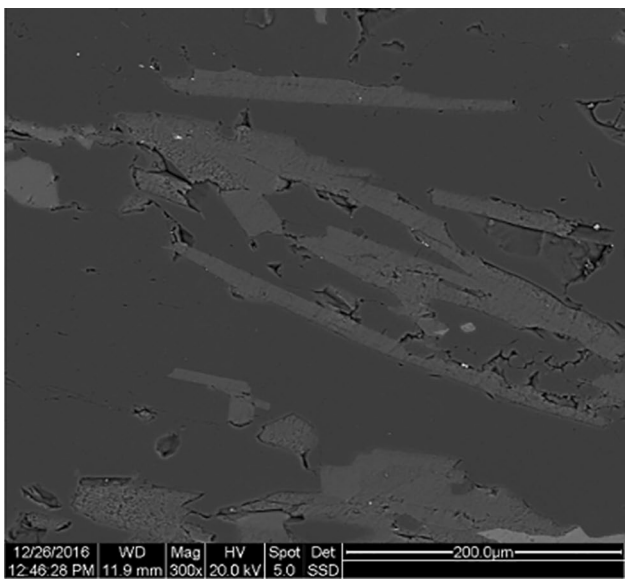

Fig. 5 Greyscale image under ESEM

Mechanical tests and analysis

Preparation and screening of specimens

Cores with different schistose angles α (the angle between the longitudinal axis of the specimen and the schistosity planes) were drilled and made into cylindrical specimens (a portion of the specimens are shown in Fig. 6) with a diameter of 50 mm and a height of 100 mm. The upper and lower end faces of the specimens were ground and polished to a roughness error less than 0.2 mm to keep the end faces of the specimens parallel to each other. Efforts were made to select qualified specimens to eliminate accidental errors in the subsequent mechanical test results as much as possible. The specimens with cracks on the surface were first screened out, and some specimens with $\alpha = 0°$, 20°, 30°, 60° and 90° were tentatively obtained.

All specimens were dried in an oven at 105 °C for 24 h, and then the P-wave velocity test was carried out by a ZBL-U520 nonmetallic ultrasonic detector. The frequency of the P-wave transducer was set at 50 kHz, and the sampling interval was 0.1 μs. Before the test, an appropriate amount of Vaseline was applied between the transducer and the end face of the specimen to ensure the signal stability of the system. Based on the principle that specimens with the same schistose angle should have similar P-wave velocities,

Fig. 6 Schist specimens

the specimens with irregular cracks inside, whose P-wave velocities usually differ greatly from the mean value of the specimens with the corresponding angle α, were discarded. From the results, the wave velocity of the selected specimens changes as a function of the schistose angle. The minimum value at $\alpha = 90°$ reaches 2785.0 m/s, and the P-wave velocity increases with decreasing schistose angle. The maximum value is as high as 5251.6 m/s at $\alpha = 0°$. The trend of the P-wave velocity is consistent with the test results of Kim et al. (2012) and is strongly dependent on the microstructure of the sample (Yin et al. 2020).

The selected dry specimens were divided into four groups, and each group contained specimens with $\alpha = 0$–$90°$. Then, three groups were soaked in different ways: (1) natural water immersion for 1 day (state 2), (2) natural water immersion for 1 week (state 3) and (3) water immersion under vacuum for 1 month (state 4). Then, the four groups of specimens, including one dry group (no. S1) and three groups (nos. S2–S4) soaked in water for different durations, were subjected to uniaxial compression using an RMT-401A rock and concrete mechanical test system.

Test results and analysis of dry specimens

Stress–strain curves

The strong brittleness of the dry specimens is revealed by the strain softening characteristics of the stress–strain curves of the dry group (Fig. 7). According to the shape of the curves, all the specimens with different schistose angles have gone through the compaction stage, linear elastic stage and nonlinear deformation stage before encountering the peak stress. The main differences are as follows. (1) The specimens with $\alpha = 90°$ and 60° experience more prominent compaction than those with other schistose angles, while the specimen with $\alpha = 0°$ presents relatively insignificant compaction. (2) The curve of the specimen with $\alpha = 0°$ exhibits obvious oscillation and fluctuation near the peak point; this is nonexistent or inconspicuous in the specimens with other schistose angles. (3) In the linear elastic stage, the distinct slopes of the curves for different specimens suggest that the elastic modulus of the schist varies with the loading direction. The value of the schist loaded parallel to the schistosity planes ($\alpha = 0°$) is conspicuously larger than that loaded perpendicular to the schistosity planes ($\alpha = 90°$).

Strength anisotropy

It is recognized that the progressive deformation and fracture failure of brittle rock under compression are always accompanied by crack propagation and evolution. In this process, the response of the mechanical behaviour of rock can be interpreted well by the stress–strain curve. According to Bieniawski (1967), Eberhardt et al. (1998) and Diederichs et al. (2004), nearly homogeneous brittle rock usually goes through four stages before failure, in accord with the shape change of the stress–strain curve (Fig. 8).

Compaction stage (I). In the initial stage, the original defects (such as intergranular pores and microcracks) compressed by the axial stress in rock tend to close, which leads to the gradual compaction of the rock. As a response, initial nonlinear deformation arises in rock. In this stage, the axial stress–strain curve is commonly characterized by concave bending.

Linear elastic stage (II). Once the axial stress reaches the crack closure strength (σ_{cc}), the rock can be regarded as a linear elastic material. Correspondingly, the axial stress acting on the rock increases linearly with the axial strain.

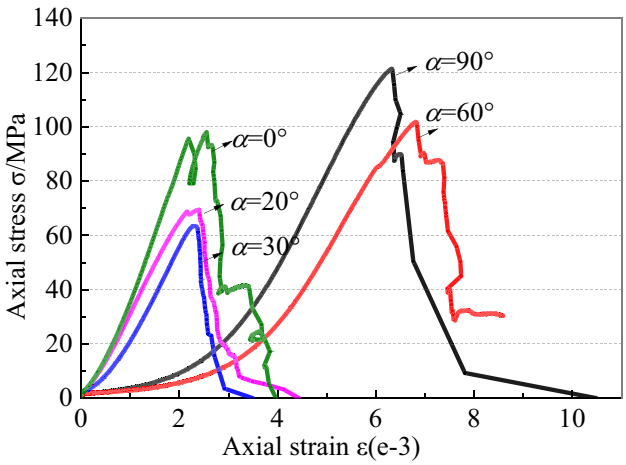

Fig. 7 Stress–strain curves of dry specimens

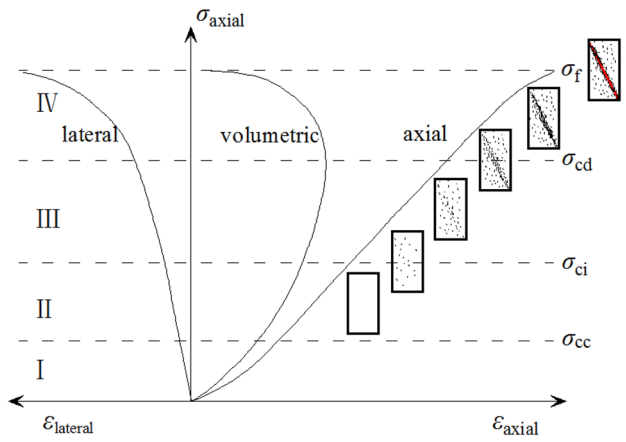

Fig. 8 Typical stress–strain curves and progressive failure process of brittle rock (according to Brace et al. 1966; Bieniawski 1967; Eberhardt et al. 1998)

Stable crack growth stage (III). Stress concentrations are apt to appear at the locations of the original defects. The stresses in these areas can even be several orders of magnitude higher than the far-field stress (Peng and Johnson 1970). Once the axial force increases to the elastic limit value, the concentrated stress value exceeds the strength of the material at the defect position, leading to the initiation of new cracks. The corresponding critical axial stress is called the crack initiation strength (σ_{ci}) of the rock. After this, irrecoverable deformation appears in the rock material, and the axial stress–strain curve presents nonlinear characteristics. After the appearance of new cracks, a characteristic phenomenon is observed; that is, the change rate of the transverse strain increase is larger than that of the axial strain increase, indicating that the lateral expansion of the rock develops rapidly. Thus, it is believed that the new crack is the product of the concentrated tensile stress and that the tensile crack generally develops along the axial force direction. The initial developing cracks are commonly considered stable cracks because they increase in number and expand in size only under the condition of increasing load.

Accelerated crack growth stage (IV). When the axial stress reaches the damage strength (σ_{cd}) of rock, the volume strain reaches the maximum, and then independent cracks begin to coalesce and interact, leading to the unstable development of cracks. In this stage, the internal structure of rock changes most significantly, and the crack density even increases by more than 7 times (Hallbauer et al. 1973). The gradually coalesced cracks eventually connect with each other and form a fracture plane through the rock, which represents the occurrence of rock failure, accompanied by the appearance of the peak point of the stress–strain curve.

The deformation resistance of the rock is weakened due to the continuous damage caused by newly developed cracks, resulting in a nonlinear increase in stress with strain. In the process of crack evolution from crack initiation to rock failure, there are several stress thresholds corresponding to the critical strength of rock, namely, the crack initiation strength (σ_{ci}), damage strength (σ_{cd}) and failure strength (σ_f). It has been proven that the failure strength is not an index reflecting the property of the material itself due to its close dependence on the loading rate and the size of the specimen (Hudson et al. 1972; Martin and Chandler 1994). Associated with the transient strain hardening effect of specimens, it is an unreliable value under long-term loading (Martin and Chandler 1994). However, this index is still widely used to establish the strength envelope and further obtain basic shear strength parameters to support the stability analysis and design of geotechnical engineering. The crack initiation strength and damage strength correspond to the initiation of new cracks and the onset of the unstable propagation of cracks in rock, respectively. They reflect the properties of the material, independent of the size of the specimen (Martin and Chandler 1994). The crack initiation strength, protected from the number of loading cycles, is controlled by the fracture toughness and the nature of defects such as pre-existing cracks. The corresponding crack initiation stress is located at the end point of linear elasticity in the axial stress–strain curve, which can be relatively precisely determined. The damage strength is considered a reliable index of the long-term strength of rock and changes sensitively with the cyclic damage degree (Park and Bobet 2010). The difference in the damage degree in the original specimens has a strong influence on the test results, and more reliable means are needed to effectively determine the critical strength. Here, we investigate only the anisotropy of the crack initiation strength and failure strength as well as the corresponding energy anisotropy.

A variety of methods have been proposed to determine the crack initiation strength of rock, such as the lateral strain difference, crack volume strain, axial strain and axial stiffness method. Among them, some methods produce larger artificial errors, while some need more data to achieve higher accuracy. The axial stiffness is a simple method proposed by Eberhardt et al. (1998) based on the understanding of the trend of the axial stiffness with stress. Yin et al. (2020) further utilized the moving average method and linear fitting to process the monitored axial stress–strain data to more accurately determine the crack initiation strength corresponding to the upper limit point of the linear elastic section in the axial stress–strain curve on the basis of the axial stiffness method. The crack initiation strength of schist specimens was determined with this improved method.

The failure and crack initiation strength were plotted as a function of the schistose angle (Fig. 9). This shows that both critical strengths vary in a U-shaped manner with the schistose angle. The minimum value occurs at $\alpha = 30°$, while

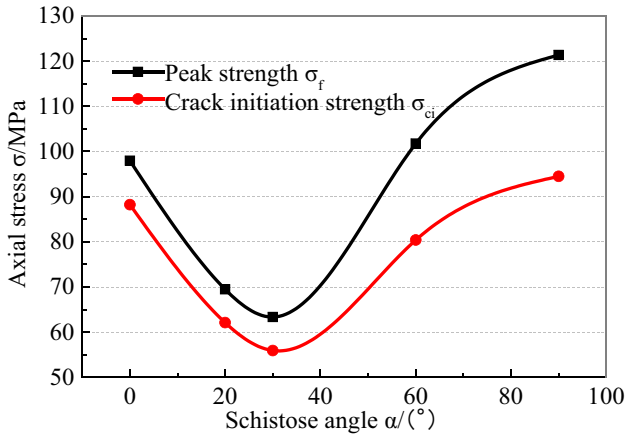

Fig. 9 Critical strength variation of dry specimens with schistose angle

the maximum occurs at $\alpha = 90°$. Here, strength anisotropy is quantified as the ratio $S_{f(ci)}$, which is expressed as follows:

$$S_{f(ci)} = \frac{\sigma_{f(ci)}^{max}}{\sigma_{f(ci)}^{min}} \tag{1}$$

where $S_{f(ci)}$ represents the anisotropy degree measured by failure strength or crack initiation strength. $\sigma_{f(ci)}^{max}$ and $\sigma_{f(ci)}^{min}$ repressent the maximum and minimum values of the failure strength or crack initiation strength among the dry specimens with different schistose angles, respectively.

As a result, the anisotropy ratios of the failure strength (S_f) and crack initiation strength (S_{ci}) are 1.92 and 1.69, respectively. According to the classification of the anisotropy grade (Table 1; Rc is the ratio of maximum and minimum uniaxial compressive strength) by Ramamurthy (1993), the quartz mica schist tested in this study is a low level anisotropic rock.

Energy anisotropy

Before the loss of its bearing capacity, rock goes through the generation, expansion and connection of new cracks in turn. The growth of new cracks continuously absorbs energy, and the sliding friction between the surfaces of cracks inevitably dissipates energy. This suggests that the deformation and failure of rock is always accompanied by energy accumulation and dissipation. When a rock subjected to an external mechanical compression force reaches the peak stress, part of the external work is converted into irreversible dissipation energy and the other into recoverable elastic energy. The dissipation of energy is closely associated with the loss of cohesion in the microstructure of rock (Xie et al. 2005). Elastic energy can be released after unloading the compression force on rock, which is the internal cause of sudden rock failure (Xie et al. 2005). According to the law of the conservation and transformation of energy, the total strain energy U provided per unit volume rock under compression is divided into elastic strain energy U^e and dissipation energy U^d, and their relationship is shown in the stress–strain curve in Fig. 10. The area of the shadow part enclosed by the unloading curve and the abscissa axis represents the releasable elastic energy U^e, while the area of the blank part enclosed by the loading curve, the unloading curve and the abscissa axis is the irrecoverable dissipation energy U^d. The area enclosed by the loading curve and the abscissa axis is equal to the total energy U. The three kinds of energies adhere to the following formula:

$$U = U^d + U^e \tag{2}$$

In the complex stress state, the total energy and elastic energy of the rock specimen in principal stress space can be expressed as:

$$U = \int \sigma 1 d\varepsilon 1 + \int \sigma 2 d\varepsilon 2 + \int \sigma 3 d\varepsilon 3 \tag{3}$$

$$U^e = \frac{1}{2}\sigma 1 \varepsilon_1^e + \frac{1}{2}\sigma 1 \varepsilon_2^e + \frac{1}{2}\sigma 1 \varepsilon_3^e \tag{4}$$

where $\sigma 1$, $\sigma 2$ and $\sigma 3$ represent the maximum, intermediate and minimum principal stresses, respectively. $\varepsilon 1$, $\varepsilon 2$ and $\varepsilon 3$ represent the corresponding principal strains. ε^e represents the elastic strain.

Table 1 Grade division of strength anisotropy (Ramamurthy 1993)

Anisotropy level	Anisotropy ratio *Rc*
Isotropy	$1.0 < Rc \le 1.1$
Low anisotropy	$1.1 < Rc \le 2.0$
Medium anisotropy	$2.0 < Rc \le 4.0$
High anisotropy	$4.0 < Rc \le 6.0$
Very high anisotropy	$6.0 < Rc$

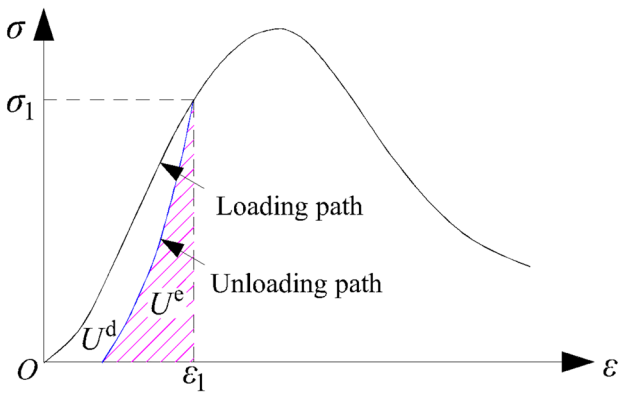

Fig. 10 Energy characterization of rock during compression

Table 2 Energy values of dry specimens at the critical stress points

Critical stress point	Energy type	Energy values of specimens (kJ/m^3)				
		$\alpha=0°$	$\alpha=20°$	$\alpha=30°$	$\alpha=60°$	$\alpha=90°$
Crack initiation point	U_*^e	73.34	51.71	45.65	102.73	126.46
	U_*^d	3.56	1.98	2.29	25.71	19.62
	U_*	76.90	53.69	47.94	128.44	146.08
Peak point	U^e	93.64	65.66	59.58	159.19	207.24
	U^d	35.03	22.68	6.23	56.52	44.35
	U	128.67	88.34	65.81	215.71	251.59

U^e (U_*^e), U^d (U_*^d) and U (U_*) represent the elastic, dissipation and total element strain energy, respectively

For a uniaxial compression test, since only the axial load does work in the whole loading process, the strain energy can be obtained by integrating the axial stress–strain curves. Therefore, the total energy and elastic energy can be easily calculated by the following expressions:

$$U = \int \sigma 1 \mathrm{d}\varepsilon 1 \tag{5}$$

$$U^e = \frac{1}{2}\sigma 1 \varepsilon_1^e = \frac{1}{2E_u}\sigma_1^2 \tag{6}$$

where E_u is the unloading elastic modulus.

However, the unloading modulus of elasticity cannot be obtained directly from the continuous loading stress–strain curve. It is generally considered that the slope of the straight-line section of the unloading curve is approximately the same as that of the loading curve (Liang et al. 2015). Thus, the loading elastic modulus E is used instead of the unloading elastic modulus E_u, and the elastic energy can be approximately expressed as follows:

$$U^e = \frac{1}{2E}\sigma_1^2 \tag{7}$$

The element strain energies of dry specimens at the points of crack initiation stress and peak stress are calculated with Eqs. (2), (5) and (7), respectively, and the results are shown in Table 2. The energy variation of the dry schist with schistose angle at two critical stress points is exhibited in Fig. 11, clearly revealing the orientation dependence of the energy. The elastic energy and total energy decrease first and then increase with increasing schistose angle at the crack initiation and peak points. The minimum value occurs at $\alpha=30°$, and the maximum occurs at $\alpha=90°$. The dissipation energy fluctuates with the changing schistose angle, and the lowest point is almost at $\alpha=30°$. At both the crack initiation point and peak point, the elastic, dissipation and total energies of the specimens in the range of $\alpha=0$ to 30° are significantly lower than those in the range of $\alpha=60$ to 90°.

The orientation effect on the energy change from crack initiation to failure of schist deserves close attention. The data shown in Table 2 reveal that the dissipation energy at the crack initiation point is much lower than that at the peak

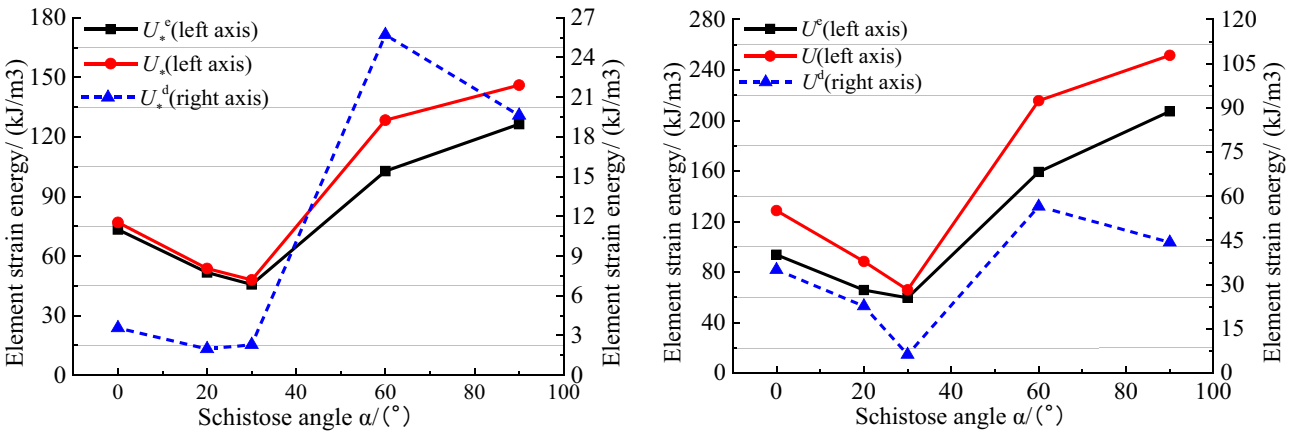

(a) at the crack initiation stress point

(b) at the peak stress point

Fig. 11 Energy variation of dry specimens with schistose angle at the critical stress point: (**a**) at the crack initiation stress point; (**b**) at the peak stress point

point, while the difference in elastic energy is relatively small. The increment of the dissipation energy at the peak point relative to the crack initiation point is only 3.94 kJ/m^3 at $\alpha = 30°$, much less than that of other specimens (31.47, 20.70, 30.81 and 24.73 kJ/m^3, respectively, from $\alpha = 0$ to 90°). The energy increment of each specimen from crack initiation to failure was compared, and it is concluded that the ratios of the dissipation energy increment to the elastic energy increment of $\alpha = 0°$ and 20° (1.55 and 1.48) are significantly larger than those of $\alpha = 30°$, 60° and 90° (0.28, 0.55 and 0.31, respectively). This suggests that most of the input energy is dissipated in the stage of crack propagation when loading nearly parallel to the schistosity planes, while the input energy is still mainly converted into elastic energy and stored in this stage when loading oblique or vertical to the schistosity planes. Note that both the increment of elastic energy and that of dissipation energy are considerable for specimens with $\alpha = 60$–90°. The above characteristics are closely related to the failure modes of the schist specimens, which is explained in detail in the "Discussion" section.

From the perspective of energy, the deformation and failure of rock under compression is a process of energy input, elastic energy accumulation and energy dissipation. To further analyse the influence of the schistose angle on the internal energy allocation mechanism, the ratio of elastic energy to total energy of each dry specimen was calculated, and the variation in the energy ratios at the crack initiation point and peak point with the schistose angle was plotted, as shown in Fig. 12. The curves fluctuate as a function of schistose angle, and the fluctuation shapes are opposite to those of the curves of dissipation energy in Fig. 11. At the crack initiation point, the energy ratios of specimens with $\alpha = 0$–30° are significantly larger than those with $\alpha = 60$–90°, which corresponds well with the differences between the stress–strain curves in the compaction stage. This suggests that with the change in the loading direction, the more obvious the compaction phenomenon is,

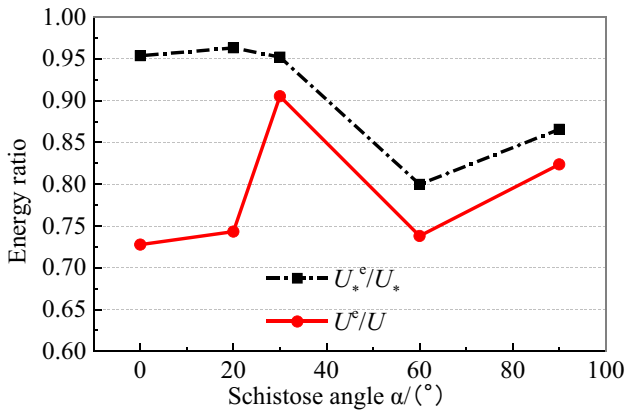

Fig. 12 Variation of energy ratios at crack initiation point and peak point with schistose angle

the smaller the ratio of elastic energy to total energy at the crack initiation point. This is because in the compaction stage, the input energy is almost dissipated and cannot be stored in rock, accompanied by the irrecoverable deformation of the specimen. At the peak point, the energy ratio increases gradually from $\alpha = 0°$ to 30° and reaches a maximum at $\alpha = 30°$. In addition, the energy ratio of the schist is as high as 0.80–0.96 at the crack initiation point, which is significantly larger than that at the peak point. Because the input energy is largely converted into elastic energy storage in the stage of linear elastic deformation, a large increase in dissipation energy occurs in the process from the initiation of new cracks to the occurrence of failure. During this period, the proportion of elastic energy tends to decrease.

The above characteristics indicate that the quartzite mica schist has obvious energy anisotropy under uniaxial compression. The rock loaded at 30° to the schistosity plane exhibits the least energy consumed for crack propagation (Fig. 11), and the final accumulated energy ratio of the specimen with $\alpha = 30°$ is much higher than those of specimens with other schistose angles (Fig. 12). Under loading nearly perpendicular to the schistosity planes, the schist must be subjected to higher external work to be damaged. Despite the high energy loss for rock damage, the input energy is converted more into elastic energy to be stored. Once the energy storage limit of the rock is exceeded, brittle failure occurs, and local rock fragments can even fly out sometimes due to the rapid release of stored elastic energy, which has been confirmed by a large number of laboratory test phenomena. Rock bursts often occur in deep underground engineering construction in brittle rock areas. This geotechnical engineering disaster is closely related to energy conversion. When the elastic energy accumulated in the rock mass exceeds the limit of energy storage under the new stress state after excavation, part of the surplus energy is transferred, and part of the energy is released suddenly and violently, resulting in rock burst. The above test results reveal that the occurrence position of rock bursts is closely dependent on the dip angle of the weak planes in the surrounding rock. Specifically, the position where the maximum principal stress is perpendicular to weak planes tends towards rock bursts, and rock bursts are less likely to occur at the position where the maximum principal stress is oblique to the weak planes at 30°.

Test results and analysis of water-immersed specimens

Stress–strain curves

Since the schistose angles corresponding to the maximum and minimum critical strengths have been found, we focus on the mechanical performance of specimens with $\alpha = 90°$, 30° and 0° to explore the influence of water on the strength anisotropy of the schist. The axial stress–strain curves of

specimens with $\alpha = 90°$, 30° and 0° in four water immersion states (the dry state is taken into account) are shown in Fig. 13. Some common mechanical properties are revealed as follows:

(1) The slope variation of the linear elastic stage in the curves of Fig. 13 indicates that when the water-bearing state changes from dry to saturation, the elastic modulus of the sample decreases gradually. (2) After entering the plastic yield stage, the dry specimen reaches the peak strength rapidly, and then the stress drops sharply, showing brittle failure characteristics. In contrast, the segments of plastic yield and post peak of the curves for the water-immersed specimens develop relatively slowly, indicating that the ductility of the specimens is enhanced to a certain extent by the influence of water.

In addition, the curves of the specimens with $\alpha = 90°$, 30° and 0° display specific performance. Despite a local anomaly (S2), the increasing trend of the peak strain of the specimen with $\alpha = 90°$ is still noticeable with increasing immersion time (Fig. 13a). As shown in Fig. 13b, in contrast to the dry state, the post-peak curves of the water-immersed specimens with $\alpha = 30°$ display a certain fluctuation, and the stress decreases gradually, accompanied by the obvious appearance of residual strength. Figure 13c displays the characteristics of a small change range for the strain values at the peak point with the various water immersion states and the oscillation fluctuation phenomenon in the peak value and post peak for all curves.

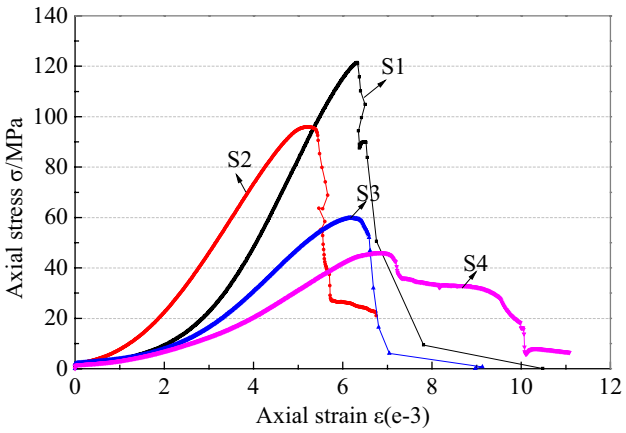

(a) α=90°

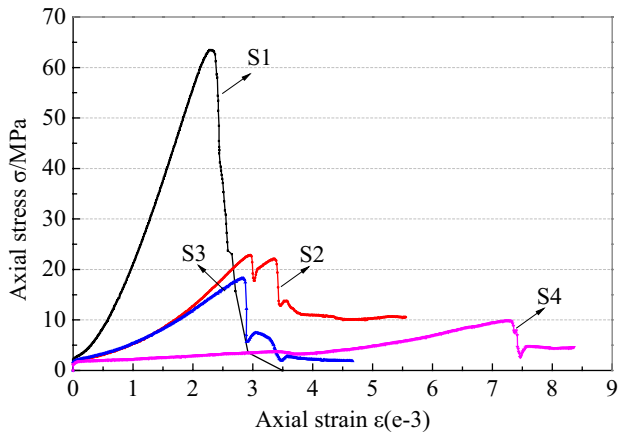

(b) α=30°

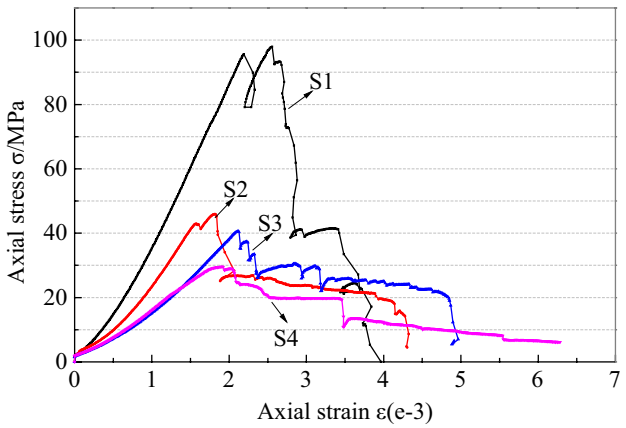

(c) α=0°

Fig. 13 Stress–strain curves of specimens in different water immersion states: (**a**) $\alpha = 90°$; (**b**) $\alpha = 30°$; (**c**) $\alpha = 0°$ (S1, dry state; S2, natural immersion for 1 day; S3, natural immersion for 1 week; S4, immersion in vacuum for 1 month)

Strength anisotropy

The failure strength and crack initiation strength of the specimens in different water immersion states were determined and are shown in Table 3. Both critical strengths of the specimens with specific schistose angles decrease gradually with increasing immersion time, revealing an obvious water softening effect. The strength reduction rate was used to quantitatively measure the softening degree of specimens with the same schistose angle. The expression is as follows:

$$R_{\mathrm{f(ci)}} = \frac{\sigma_{\mathrm{f(ci)}}^{\mathrm{smax}} - \sigma_{\mathrm{f(ci)}}^{\mathrm{smin}}}{\sigma_{\mathrm{f(ci)}}^{\mathrm{smax}}} \tag{8}$$

where $R_{\mathrm{f(ci)}}$ represents the reduction rate of the failure strength or crack initiation strength. $\sigma_{\mathrm{f(ci)}}^{\mathrm{smax}}$ and $\sigma_{\mathrm{f(ci)}}^{\mathrm{smin}}$ represent the maximum and minimum values of failure strength or crack initiation strength among the four water immersion states, respectively.

The specimens with $\alpha = 90°$, 30° and 0° were compared with regard to the reduction rates of failure strength (R_{f}) and crack initiation strength (R_{ci}). The results show that $\alpha = 30° > \alpha = 0° > \alpha = 90°$ for both R_{f} and R_{ci} (Fig. 14). This suggests that the reduction effect of water on the

Table 3 Critical strengths of specimens in different water immersion states

Schistose angle α	Strength index	Critical strength of specimens				Strength reduction rate $R_{f(ci)}$
		S1	S2	S3	S4	
0°	σ_f	98.0	45.9	40.7	29.6	0.70
	σ_{ci}	88.2	34.8	30.1	20.1	0.77
30°	σ_f	63.3	22.8	18.3	9.9	0.84
	σ_{ci}	55.9	18.7	12.5	7.2	0.87
90°	σ_f	121.4	95.7	59.8	45.9	0.62
	σ_{ci}	94.5	60.4	42.4	31.6	0.67

σ_f and σ_{ci} represent the failure strength and crack initiation strength; S1–S4 represent four water immersion states

critical strength is especially significant for the specimen with $\alpha = 30°$, while the specimen with $\alpha = 90°$ has relatively poor strength sensitivity to water. For the same water immersion state, the critical strengths of specimens with different schistose angles were compared and the order $\sigma_{f(ci)}$ $(\alpha = 90°) > \sigma_{f(ci)}$ $(\alpha = 0°) > \sigma_{f(ci)}$ $(\alpha = 30°)$ is obtained. The ratio $S_{f(ci)}$ of $\sigma_{f(ci)}$ $(\alpha = 90°)$ to $\sigma_{f(ci)}$ $(\alpha = 30°)$ for the specimens in the same water immersion state was still utilized to quantitatively analyse the response of the strength anisotropy to water.

As shown in Fig. 15, in general, the strength anisotropy tends to be enhanced with increasing immersion time, which is closely related to the unequal influence degree of water on the critical strength of specimens with different schistose angles. According to the classification of rock anisotropy (Table 1), the anisotropy of schist changes from a low level in the dry state to a medium or high level after it absorbs water. In addition, the anisotropy of the failure strength is abnormally high after immersion for 1 day. By contrast, the anisotropy of the crack initiation strength exhibits a clearer trend and is superior to the failure strength with respect to reflecting the effect of water on the strength anisotropy. The anisotropy of the crack initiation strength increases obviously from the dry state to immersion for 1 day, increases slightly after immersion for 1 week and then greatly increases again after immersion in vacuum for 1 month. Such changing characteristics are not independent of the mechanism of water action.

Energy anisotropy

All the strain energy data of the specimens in different water immersion states are shown in Table 4. The energy values of the specimens with $\alpha = 90°$, 30° and 0° at the critical stress points as a function of immersion time are displayed in Fig. 16. For specimens with $\alpha = 90°$, the elastic energy and total energy at the crack initiation and peak points are negatively correlated with the immersion time (Fig. 16a), indicating that the weakening of the physico-mechanical properties of the specimen by water causes the loss of strain energy. The loss rate (*LR*) at the peak point is used to measure the water effect on the energy of the specimen in the whole process of deformation and failure. The expression is as follows:

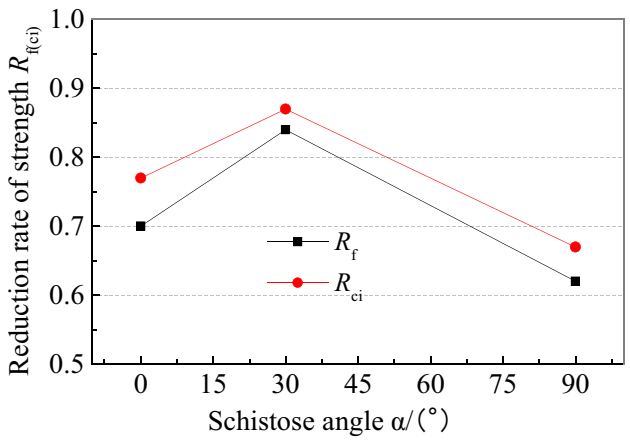

Fig. 14 Variation of reduction rates of failure strength and crack initiation strength with schistose angle

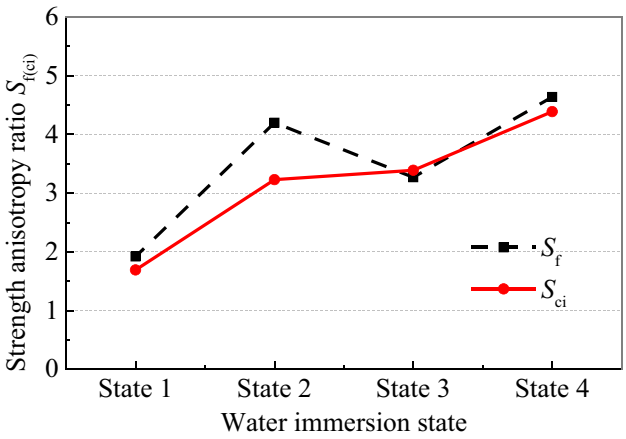

Fig. 15 Variation of strength anisotropy ratios with water immersion state

Table 4 Energy values of specimens in different water immersion states

Critical stress point	Energy type	Energy value of specimens (kJ/m^3)											
		$\alpha=0°$				$\alpha=30°$				$\alpha=90°$			
		S1	S2	S3	S4	S1	S2	S3	S4	S1	S2	S3	S4
Crack initiation point	U_*^e	73.34	17.64	21.38	13.51	45.65	17.84	9.24	10.49	126.46	75.42	54.41	44.42
	U_*^d	3.56	2.88	2.79	0.70	2.29	2.62	1.99	12.64	19.62	12.54	14.10	13.79
	U_*	76.90	20.52	24.17	14.21	47.94	20.45	11.22	23.13	146.08	87.96	68.51	58.22
Peak point	U^e	93.64	30.29	37.08	24.93	59.58	26.31	21.97	16.12	207.24	163.00	104.21	94.84
	U^d	35.03	10.05	2.91	4.67	6.23	3.00	2.89	16.79	44.35	48.54	42.75	43.81
	U	128.66	40.34	39.99	29.60	65.81	29.31	24.86	32.91	251.59	211.54	146.96	138.65

U^e (U_*^e), U^d (U_*^d) and U (U_*) represent the elastic, dissipation and total energy, respectively; S1–S4 represent four water immersion states

$$LR^{(e)} = \frac{U_{smax}^{(e)} - U_{smin}^{(e)}}{U_{smax}^{t(e)}} \tag{9}$$

where $LR^{(e)}$ represents the loss rate of total energy or elastic energy at the peak point and $U_{smax}^{(e)}$ represents the maximum total energy or elastic energy at the peak point among the four water immersion states. Correspondingly, $U_{smin}^{(e)}$ represents the minimum energy.

The loss rates of elastic energy (LR^e) and total energy (LR) of the dry specimen with $\alpha=90°$ can reach 0.54 and 0.45, respectively, after long-term water saturation. The curves of dissipation energy fluctuate unevenly, and its slight change with increasing immersion time (Fig. 16a) indicates that the dissipation energy of the specimen with $\alpha=90°$ is relatively insensitive to the water effect.

Under the effect of water, the elastic energy of the specimen with $\alpha=30°$ at two critical points decreases gradually (Fig. 16b). From the dry state to the beginning of immersion (for 1 day and 1 week), the total energy tends to decrease but increases after long-term immersion (for 1 month). This energy performance is attributed to the appearance of significant compaction and large peak strain (Fig. 13b) for the specimen affected by water for a long time. As shown in Fig. 16b, at the beginning of immersion, the dissipation energy decreases as a whole. However, after 1 month of immersion, this energy increases greatly, which contributes to the trend of the total energy. For the specimen with $\alpha=30°$ suffering from the water effect, LR^e and LR are 0.73 and 0.62, respectively.

Except for the dissipation energy at the peak point increasing to a certain extent after long-term immersion, the energy values of the specimen with $\alpha=0°$ at the critical points decrease with increasing immersion time (Fig. 16c). By comparing the change characteristics of the dissipation energy curves with the two critical points, we can conclude that the influence of long-term immersion on the specimen with $\alpha=0°$ is mainly concentrated in the crack propagation stage from the perspective of progressive failure. LR^e and LR are 0.73 and 0.77, respectively.

The loss rates of the elastic energy (LR^e) and total energy (LR) for specimens with $\alpha=0°$ and 30° are significantly higher than that for the specimen with $\alpha=90°$ under the action of water, indicating that the energy change of the former two is more sensitive to water than that of the latter, and the water effect is more significant for the specimens with $\alpha=0°$ and 30°. The difference between the energy trends of short-term and long-term water immersion reveals that the microstructure of rock subjected to the continuous action of water is likely to change in a critical period and is closely related to the mechanism of the water effect.

In addition, the energy storage limit of the specimens decreases gradually with increasing immersion time. After the peak stress point, the failure rate of rock experiencing the water effect decreases remarkably due to the large reduction in the elastic energy originally accumulated to promote the subsequent failure and is even insufficient to supply the energy for the complete independent failure of the rock. Thus, external energy provided by machinery is needed to supply energy for the subsequent failure. This is the reason why the stress gradient decreases and the residual strength phenomenon occurs after the peak point in the stress–strain curve of the specimen affected by water. In practical engineering, the prevention of rock bursts by injecting water into the rock stratum essentially makes use of the response of rock energy to water.

The ratio of the elastic energy to total energy of the specimens in the four water immersion states was calculated, and the energy ratios at the crack initiation point and peak point as a function of immersion time are shown in Fig. 17. The energy ratios of specimens with $\alpha=90°$ and 30° decrease gradually with increasing immersion time at both the crack initiation and peak points. This suggests that for these two specimens, the effect of water on the

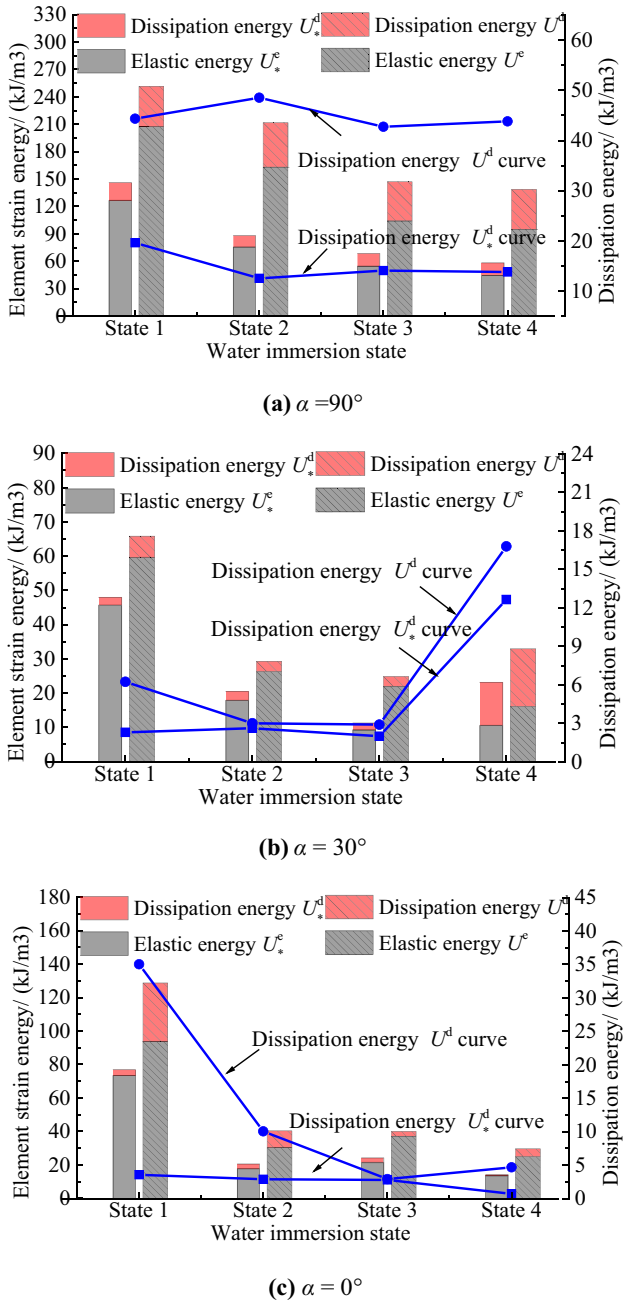

Fig. 16 Energy variation of specimens with water immersion state: (**a**) $\alpha = 90°$; (**b**) $\alpha = 30°$; (**c**) $\alpha = 0°$ (the bars correspond to the left axis, and the curves correspond to the right axis)

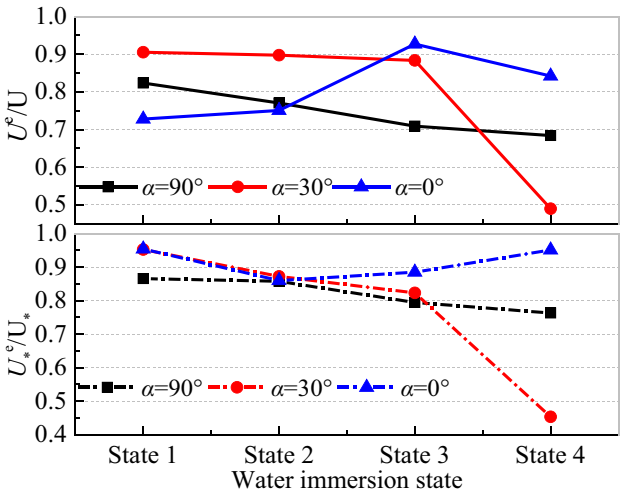

Fig. 17 Variation of energy ratios of specimens at crack initiation and peak points with water immersion state

energy storage limit is stronger than that on the energy dissipation.

At $\alpha = 90°$, the slopes of the two energy ratio curves tend to decrease gradually. Combined with the energy variation in Fig. 16a, it can be concluded that the water immersion time effect on the elastic energy gradually weakens or even disappears. As a result, the elastic energy and energy ratio at the two critical points are likely to eventually maintain constant values.

At $\alpha = 30°$, the energy ratios at the two critical points decrease slowly from the dry state to immersion for 1 week, and the ratio curves suddenly drop sharply after immersion in vacuum for 1 month, which is caused by the significant increase in the energy dissipation of the specimen in this state. Further study is still needed to determine the change trend of the energy ratio when the specimen is soaked for a longer time.

At $\alpha = 0°$, the energy ratios, which are not sensitive to immersion time, are basically maintained at approximately 0.9 at the crack initiation point, indicating that water has a weak influence on the compaction stage from the perspective of progressive failure of the specimen. At the peak point, it reveals a more significant effect of water on dissipation energy than on elastic energy at the beginning of immersion, which leads to a gradual increase in the energy ratio of the specimens from the dry state to immersion for 1 week. However, after long-term immersion, the energy ratio appears to decrease accompanied by an increase in dissipation energy.

Discussion

The controlling effect of fabric on anisotropy

Failure modes of schist

At the critical points in the process of progressive failure, the schist displays obvious anisotropy with regard to strength and energy. This is closely related to the failure mode of the rock but essentially responds to the characteristic microstructure. In terms of the mineral distribution, flaky muscovite minerals are interbedded with granular

minerals such as feldspar and quartz, and muscovite with significant orientation tends to gather near the schistosity planes. In the defect distribution, the majority of microcracks directionally extend along the edge of the clustered muscovite minerals, while small pores are randomly distributed among the granular mineral particles. In a previous study (Yin et al. 2020), combined with the rock fabric, we discussed the failure modes of quartz mica schist subjected to uniaxial compression from the perspective of the rock macroscopic failure morphology and microscopic crack propagation mechanism, which is summarized as follows:

When schist is loaded nearly parallel to the schistosity planes (α is close to 0°), tensile-splitting failure along the weak planes appears at the macro-level (Fig. 18a). Tensile stress concentration at the tip of the oriented microcracks easily occurs in the specimen without lateral restraint, which leads to the origination of new cracks. The increasing axial stress provides external work for these cracks to grow along the edge of clustered flaky minerals and finally forms several macroscopic fracture surfaces along the schistosity planes (Fig. 18a). With the gradual appearance of these fracture surfaces, the medium material between the surfaces continues to bear the axial load until buckling of these "compression bars". The stress–strain curve of the specimen exhibits obvious fluctuations and oscillations near the peak point due to the gradual development of multiple fracture surfaces and the progressive exertion of the ultimate bearing capacity of the compression bars.

When schist is loaded obliquely with the schistosity planes at a small angle (in general, $20° < \alpha \leq 45°$), shear-slip failure along the weak planes appears at the macro-level (Fig. 18b). At the crack initiation point, sliding-tension cracking occurs along the surfaces of oriented microcracks near the clustered muscovite minerals. Due to the large specific surface area and smooth edge surface of the flaky minerals, the clustered muscovite layer provides quite weak resistance to tensile and shear failure, resulting in rapid propagation of new cracks along the weak layer (Fig. 18b). In this case, from the initiation of new cracks to the failure of the specimen, there is no gradual coalescence of a large number of cracks, and the interaction between cracks is not as intense as that of nearly homogeneous brittle rock.

When compression force is applied to schistosity planes at a large angle (in general, $\alpha > 45°$), shear failure occurs at an oblique angle with the weak planes at the macro-level (Fig. 18c). Different from the above two modes, directional microcracks no longer control the appearance of new cracks, and crack initiation mainly occurs at the ends of intergranular pores and the contact between rigid granular minerals and flexible flaky minerals. Despite the strong heterogeneity, the progressive failure of the specimen follows the typical crack evolution trend of nearly homogeneous rock. It undergoes the process from crack initiation to stable growth of independent cracks, gradual accumulation of large numbers of cracks, unstable propagation of interacting cracks and formation of a unified fracture surface by crack connections. Although the same macroscopic failure pattern appears in the specimens with $45° < \alpha < 90°$ and $\alpha = 90°$, they display certain differences in the characteristics of microcrack growth. The cracks extending to the edge of clustered muscovite are unlikely to develop horizontally along the weak

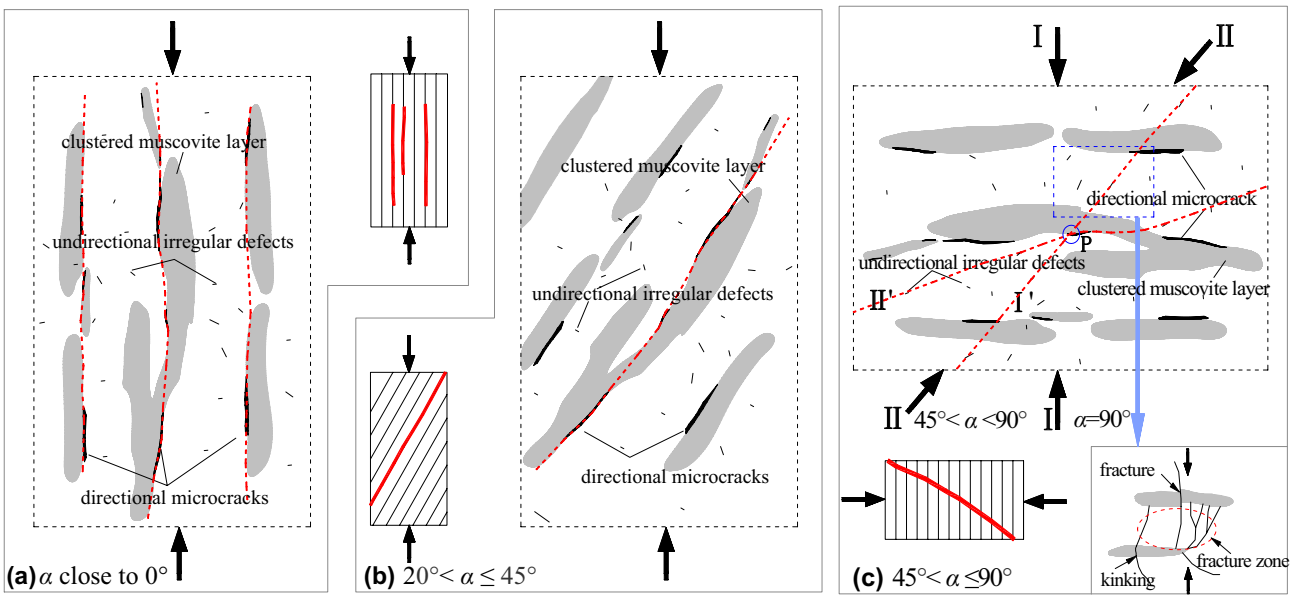

Fig. 18 Microscopic and macroscopic failure modes of schist specimens: (**a**) α close to 0°; (**b**) $20° < \alpha \leq 45°$; (**c**) $45° < \alpha \leq 90°$

plane (as shown in Fig. 18c, line I′) under loading perpendicular to schistosity planes ($\alpha = 90°$, I-I in Fig. 18c) due to the lack of tensile and shear stresses that drive cracks to propagate in this case. When the schist is loaded at a large angle inclined to the schistosity planes ($45° < \alpha < 90°$, II-II in Fig. 18c), the existence of the driving force causes the microweak planes to guide the development of cracks extending here to a certain extent (as shown in Fig. 18c, line II′). In the stage of crack growth, cracks propagating oblique to the weak planes inevitably cut off granular and flaky mineral particles, resulting in residual mineral debris on the macro-fracture surface.

When a homogeneous material with a single crack is subjected to compression, the critical stress of crack initiation varies with the angle α' between the loading direction and crack. The angle α' corresponding to the minimum critical stress is called the dominant angle of crack initiation and is usually approximately 30°. In anisotropic schist, the influence of the dominant angle is still traceable. On the one hand, when the axial force intersects with the schistosity planes at a large angle, large numbers of new cracks appear continuously at the pre-existing defects with a dominant angle, and then these cracks gradually expand and coalesce to form a macro-fracture surface with an approximate angle of 30° to the axial stress. In addition, although specimens subjected to axial force oblique to the schistosity planes at a small angle display the common shear-slip failure pattern, the specimen with $\alpha = 30°$ has the minimum crack initiation strength due to the existence of multiple microcracks with a dominant angle of crack initiation.

Figure 19 shows four groups of damaged specimens in different water immersion states. The similar distribution characteristics for the main fracture planes of the specimens with the same schistose angle suggest that although the failure mode of schist subjected to uniaxial compression strongly depends on the loading direction, it is less affected by the water immersion state. Overall, as the immersion time increases, the secondary fracture planes in the specimen with $\alpha = 90°$ decrease. Under the conditions of dry and short-term immersion, the main and secondary fracture planes intersect and cut into small rock fragments. Even flying fragments can be seen occasionally during the loading process, which does not happen with the state of long-term immersion. In the four water immersion states, the fracture planes of the specimens with $\alpha = 30°$ are almost distributed along the schistose planes. It seems that the dry specimen has a more regular and flat fracture plane along the schistose plane on the same level, but after a long immersion time, the fracture surface has a certain degree of local turning, and the roughness increases somewhat. At $\alpha = 0°$, the density of the fracture planes of schist decreases significantly with increasing immersion time, suggesting a decreasing brittleness of the specimen.

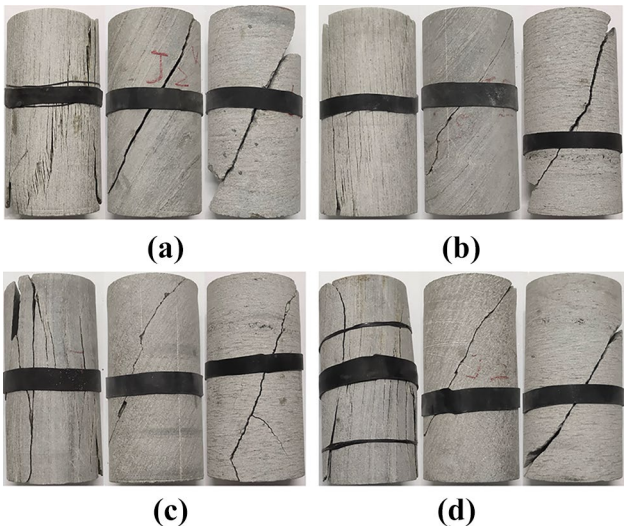

Fig. 19 Damaged specimens: (**a**), (**b**), (**c**) and (**d**) are the specimens in the states of dry, natural immersion for 1 day, immersion for 1 week and immersion for 1 month, respectively; each group of specimens corresponds to $\alpha = 0°$ and 30° and $\alpha = 90°$ from left to right

Mechanism of the strength anisotropy

In terms of the strength anisotropy, when axial compression intersects with schistosity planes at a large angle, the failure of the specimen mainly starts from cracking at the tips of intergranular pores, and a higher crack initiation strength is required to induce new cracks due to the compact mosaic of granular minerals. In the process of progressive failure, a large number of different types of cracks, such as intragranular cracks, intergranular cracks and transgranular cracks, appear gradually. A previous study revealed that at low stress levels, schist is dominated by intragranular cracks. As the stress level increases, they tend to evolve into transgranular cracks (Martin and Chandler 1994). The extended cracks cut off large numbers of mineral particles, among which hard granular minerals contribute to higher failure resistance, resulting in higher failure strength for the specimens with large schistose angles. The flaky minerals perpendicular to the compressive stress are kinked and fractured before the cracks further coalesce (Rawling et al. 2002). Since large numbers of cracks are produced in the granular mineral zone, the specimen with $\alpha = 90°$ has a wider fracture zone (Fig. 18c) than those with $\alpha = 30°$ and 0°.

When axial compression intersects with schistosity planes at a small angle, microcracks at the edge of clustered flaky minerals control the initiation of cracking. The high stress concentration at the tip of the large-scale microcracks leads to a relatively low threshold of crack initiation stress. Then, rapid propagation of new cracks is accompanied by increasing external compression associated with the poor

mechanical properties at the part of clustered minerals. As a result, the specimens with a small schistose angle have a lower failure strength.

When the loading direction is parallel to the schistosity planes, new cracks in the specimen also propagate along the weak planes. However, the mechanical mechanism of crack initiation in this case is different from that of the specimen subjected to compression oblique to the schistosity planes at a small angle. In the specimens with small angles, the surfaces of the microcracks intersect with the axial force. The microcracks are compressed and closed under the action of increasing axial stress, and slip caused by the shearing component force occurs, further triggering tensile crack initiation at the tips of pre-existing microcracks. For the specimens with angles close to 0°, the surfaces of the microcracks are nearly parallel to the axial force, and the majority of the microcracks cannot be compacted under increasing external force. Then, a large lateral strain is produced under uniaxial compression, causing concentrations of tensile stress at the tips of the microcracks. Compared with the specimens with small angles, larger axial compression is required to reach the critical lateral strain for the initiation of new cracks in this case. In addition, along with the appearance of the crack surface, the medium material between the crack surfaces acts as a vertical compression bar and can provide greater resistance before buckling. The above is the micromechanical mechanism describing the strength changing with the schistose angle in a U shape.

Mechanism of the energy anisotropy

From the perspective of energy anisotropy, when axial compression intersects with the schistosity planes at a large angle, in the initial stage of deformation, open microcracks are easily compressed and closed, and the input energy is almost completely dissipated. With the linear elastic deformation of the specimen, a large amount of elastic energy reserves reach a high critical value, which can drive crack initiation at the ends of defects, such as intergranular pores. After that, complex crack evolution involving stable and accelerated crack growth accompanies considerable energy dissipation in this process. In the stage of stable crack growth, a high elastic energy ratio is still needed to provide enough energy to drive the crack to cut off the mineral particles. The deformation and failure of the specimen with a large schistose angle develop relatively slowly, and a larger axial strain is produced before failure (Fig. 7). Additionally, mineral particles provide considerable resistance to failure, which allows the specimen to have a higher energy reserve. For these reasons, the schist specimen with a large schistose angle shows higher dissipation energy, elastic energy and total energy at the critical strength points.

When axial compression intersects with the schistosity planes at a small angle, the pre-existing microcracks are prone to generating new cracks. Moreover, the cracks rapidly expand and connect to form a unified fracture surface along the microweak plane during the crack evolution stage. As a result, elastic energy cannot be stored in large quantities in the specimen, and the energy used for crack propagation is relatively low. Especially at $\alpha = 30°$, the majority of microcracks have a dominant angle, leading to the lowest energy threshold for crack initiation. Thus, the specimen with $\alpha = 30°$ exhibits the lowest dissipation, elastic and total energy at the crack initiation point. In the process of crack growth, the energy dissipated with rock damage is very low due to the rapid development of a small number of cracks, which makes the proportion of elastic energy at the peak point much higher than that of specimens with other schistose angles.

When loading nearly parallel to the schistosity planes, the specimen is not fully compacted because the majority of large-scale microcracks are always in an open state. The relatively low elastic energy is enough to cause crack initiation and propagation along the weak planes. The elastic, dissipation and total energy of the specimen are lower than those of the specimen with a large schistose angle. As with the specimen with $\alpha = 30°$, new cracks propagate rapidly once they are initiated. However, before the failure of the rock, more energy is dissipated in this specimen than in the specimen with $\alpha = 30°$ due to the gradual appearance of multiple fracture surfaces distributed at different macroschistosity planes.

Water effect

Previous studies indicate that water has various effects on rocks, including the lubrication and softening of mineral particles, swelling and disintegration of rocks, ion exchange between water and the minerals of rock, acidification and oxidation of minerals, as well as hydrostatic pressure and excess pore water pressure of water on rocks (Zhou et al. 2003, 2005), which eventually weakens the mechanical properties of rock or reduces its effective strength. In this study, the tested specimens were immersed in drinking water. Chemical reactions such as acidification and oxidation are almost impossible under these conditions due to the scarcity of chemically active ions in water. In addition, the electrochemical action of ion exchange adsorption can be ignored considering the few clay minerals in schist.

After the dried schist is soaked, water enters the rock mainly along the microcracks at the schistosity planes, and lubrication and softening if the flaky minerals near the microcracks occurs, weakening the mechanical properties of the schist specimens. In general, the water absorption speed of rock changes from fast to slow with the prolongation of

the soaking time, implying that the water content increases rapidly in the initial stage and then slightly in the middle and later stages. As a result, the reduction in the mechanical properties of the specimen from lubrication and softening of water in the early stage is relatively high.

In this study, a uniaxial compression test was carried out immediately after water immersion. At the beginning of axial loading, compaction of the specimen is accompanied by the closure of voids, leading to an increase in the water pressure in the voids. Additional stress formed by a water wedge at the tip of a void is conducive to reducing the crack initiation threshold and promoting crack growth, further resulting in a change in the failure strength of the specimens.

In conclusion, the mechanical performance of immersed specimens under compression is generally affected by the physical and mechanical actions of water. The former weakens the ability of the specimen to resist deformation and failure by changing the properties of minerals, while the latter promotes the development of cracks in the specimen. With the weakening of the mechanical properties of the specimens, the total energy absorbed and elastic energy stored before failure decrease.

The weakening degree of water on the critical strength of quartz mica schist varies with the schistosity orientation. The weakening effect is stronger at $\alpha = 30°$ and is weaker at $\alpha = 90°$. The orientation dependence of the weakening effect is closely related to the failure modes of quartz mica schist. At $\alpha = 90°$, shear failure with cataclastic mineral particles occurs in the specimen. Crack initiation mainly occurs at the end of intergranular pores, and hard granular minerals such as quartz and feldspar have a dominant influence on the mechanical properties of rock. Due to the relatively insufficient water absorption capacity of small intergranular pores and the poor sensitivity of hard minerals to water, the specimen with $\alpha = 90°$ exhibits a relatively low reduction rate in the mechanical strength after immersion. At $\alpha = 30°$, shear-slip failure along the schistosity planes occurs in the specimen, and microcracks with the preferred orientation play a controlling role in crack initiation. After immersion, the lubrication and softening effect of water in the microcracks on flaky minerals and the hydraulic action on the tips of the microcracks greatly reduce the critical strength of the specimen. At $\alpha = 0°$, tensile-splitting failure along the schistosity planes occurs in the specimen. New tensile cracks first appear at the tips of directional microcracks and then gradually develop into tension fracture surfaces. Medium materials between different fracture surfaces bear compression loads until buckling. Although the physical action of water on flaky minerals also reduces the critical strength of the specimen with $\alpha = 0°$ to some extent, the strength reduction of the specimen is smaller than that of $\alpha = 30°$. This difference occurs because at $\alpha = 0°$, the medium material composed of hard granular minerals with poor water sensitivity plays a major role in bearing compression, and hydraulic action on the tip of the microcracks can be ignored considering that the microcracks cannot be compressed and closed due to the orientation promoting axial compression. In addition, the fact that the loss of the elastic and total energies of specimens with $\alpha = 0°$ and 30° affected by water are significantly higher than those of $\alpha = 90°$ is strongly dependent on the response mechanism and degree of water action to the schistosity orientation. Due to the orientation dependence of the degree of water weakening, the strength anisotropy of quartzite mica schist tends to be enhanced with increasing immersion time.

An interesting mechanical test result was found; that is, from the initial stage to the later stage of immersion, the variation in strength anisotropy is characterized by a large increase at first, a slight change and then a large increase again (Fig. 15). It is recognized that the water absorption capacity of rock generally weakens with increasing immersion time. The orientation dependence of the water weakening effect is usually in accordance with the expectation that the enhancement of the anisotropy decreases with increasing immersion time or even that the anisotropy degree ultimately remains constant. However, a remarkable deviation from expectations actually exists; that is, the anisotropy increases greatly after long-term immersion in water, which is obviously associated not only with the lubrication and softening effect of water on minerals but also with the hydraulics of water. During water immersion of the specimens, we found that the water quality varied with increasing immersion time. Figure 20a shows a comparison of the water quality after 1 month of immersion (left bottle) and at the beginning of immersion (right bottle). Obviously, turbidity can be seen in the left bottle, and some solid precipitant remains at the bottom of the bottle after 1 month of immersion. The precipitates were collected and air-dried, and then an X-ray powder diffraction test was conducted to obtain the mineral composition of the precipitates. The test results are shown in Fig. 20b. The results reveal that muscovite minerals account for the majority (76%) of these precipitates, indicating that after water enters the schist along the open microcracks, disintegration of muscovite minerals occurs due to the long-term action of water.

The disintegration of flaky minerals is a sudden phenomenon of mineral destruction that requires a relatively long critical time of water immersion. Thus, the mechanical properties of schist are dominantly influenced by the softening and lubrication effect of water in the early and middle stages of water immersion but subject to the disintegration effect in the later stage. The disintegration of minerals inevitably leads to structural damage at the schistosity planes. Consequently, the strength of the specimen

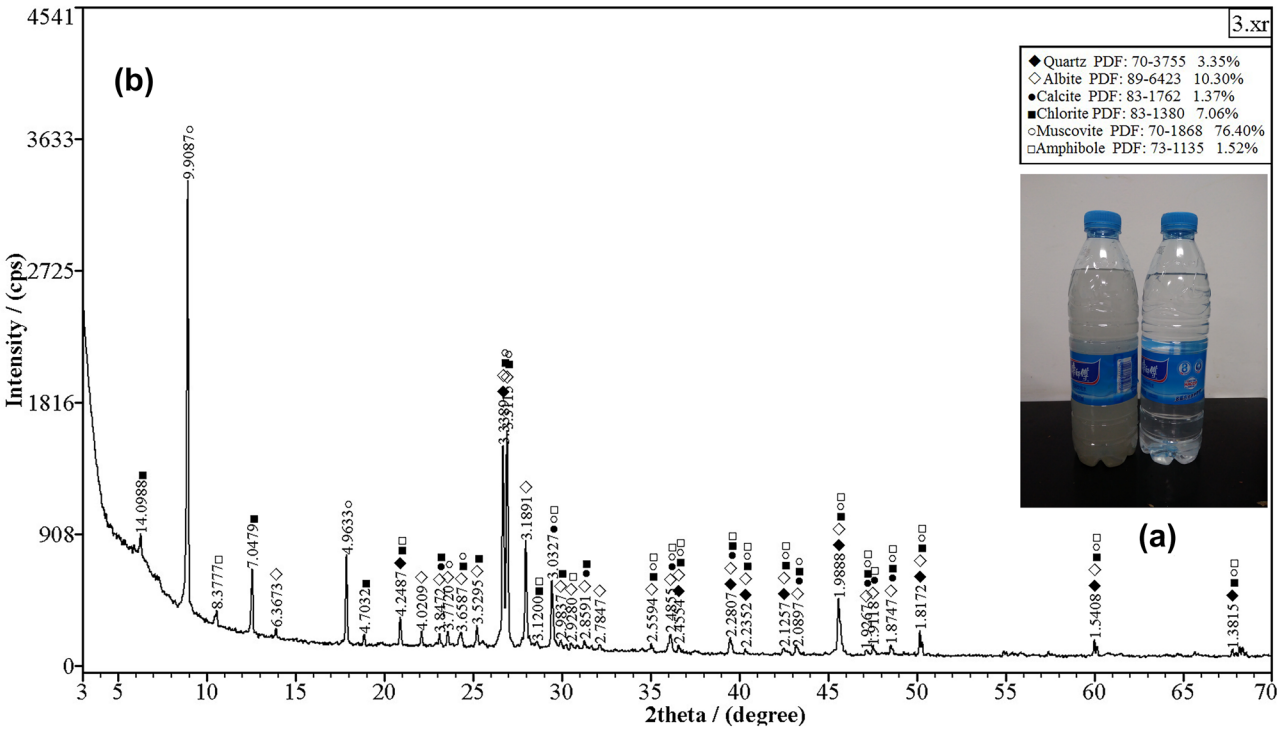

Fig. 20 Water quality and mineral composition of precipitates in water after immersion. (**a**) Comparison of water quality (**b**) Mineral composition of precipitates in water after immersion obtained by X-ray powder diffraction

($\alpha = 30°$) with slip-shear failure along the schistosity plane is greatly reduced after a long immersion. In contrast, the strength of the specimen ($\alpha = 90°$) with shear failure oblique to the schistosity planes is not strongly affected by mineral disintegration because the weak planes have little influence on the strength of the specimen. As a result, the strength anisotropy, determined by the ratio of the strength of the specimen with $\alpha = 90°$ to that with $\alpha = 30°$, increases greatly in the later stage of water immersion.

The mechanical and energy anomalies of the specimen with $\alpha = 30°$ after water immersion for 1 month are also closely related to the disintegration of flaky minerals. The structural damage caused by the disintegration of clustered muscovite is characterized by the expansion and growth of the pre-existing microcracks, which leads to a decrease in the ordering of regularly oriented microcracks near the schistosity planes. The mechanical and energy performance of the specimen ($\alpha = 30°$) with the failure characteristic of crack initiation at directional microcracks and propagation along the edge of muscovite minerals is abnormal (exhibiting phenomena such as obvious compaction, large peak strain, abnormally increased dissipation energy and total energy) due to the changed size and order of the pre-existing microcracks. The abnormal increase in the peak dissipation energy of the specimen with $\alpha = 0°$ after immersion for 1 month is also likely to be dependent on mineral disintegration.

Conclusions

In this study, four groups of cylindrical specimens with different schistose angles were prepared and subsequently dried and either soaked in water for 1 day or 1 week or soaked under vacuum for 1 month. Polarizing microscopy, environmental scanning electron microscopy, X-ray powder diffraction and uniaxial compression tests were utilized to investigate (a) the strength and energy responses of the schist to the schistosity orientation and water and (b) the micromechanism and water action mechanism of the anisotropic properties of the schist. The main conclusions are as follows:

Both the failure strength and crack initiation strength of dry schist change with the schistose angle in a U shape. Water has a significant softening effect on the strength of schist. Nevertheless, the response of schist to water differs with the schistosity orientation in terms of failure strength and crack initiation strength. Rock with $\alpha = 30°$ exhibits more sensitive strength reduction than that with $\alpha = 90°$, leading to enhanced strength anisotropy for the schist accompanied by an increasing immersion time.

The energy of the schist under compression is closely associated with the schistosity orientation. The elastic energy and total energy decrease first and then increase with increasing schistose angle. These energies reach minimum values at $\alpha = 30°$ and the maximum at $\alpha = 90°$. The energy allocation in the crack growth stage varies with the

schistosity orientation. At $\alpha = 0°$, the energy dissipated accounts for a large proportion of the total energy. In contrast, at $\alpha = 30°$, most of the external work is converted into elastic energy and stored in the rock. At $\alpha = 90°$, the schist has a stronger ability to store internal energy. Additionally, at $\alpha = 30°$, the energy dissipated for crack growth of the specimen reaches the minimum value, and the ratio of elastic energy to total energy at the peak point reaches the maximum.

In general, the total energy and elastic energy of schist decrease after immersion. However, the trend and amplitude in response to increasing immersion time vary with the schistosity orientation. At $\alpha = 30°$ and 0°, the weakening effect of water on the energy storage capacity of schist is greater than that at $\alpha = 90°$. For $\alpha = 30°$, the dissipation energy tends to decrease at the beginning of immersion but increases after long-term immersion. Similar trends are found for the dissipation energy of the specimen with $\alpha = 0°$ at the peak point. The effect of water on the energy storage limit of the two specimens with $\alpha = 90°$ and 30° is stronger than that of the energy dissipation. However, the effect is almost the opposite for the specimen with $\alpha = 0°$.

The orientation dependence of the failure mode is closely related to the characteristic microstructure of schist, which essentially controls the strength and energy anisotropy. The water effect involving the lubrication and disintegration of flaky minerals and hydraulic action has an influence on the strength and energy performance of schist. Softening and lubrication effects play a major role in the early and middle stages of water immersion. The disintegration of flaky minerals caused by prolonged immersion plays a key role in the later stage of water immersion. The hydraulic action on the tips of voids contributes to the reduction in the critical strength of specimens. Furthermore, the sensitivity of the mechanical properties to the water effect depends on the schistosity orientation, which leads to the response characteristics of the strength and energy anisotropy to water.

Funding This research is financially supported by the Natural Science Foundation of China (Grant No. 41807240) and the Nanhu Scholars Program of Xinyang Normal University and the Research Fund for the Doctoral Program of Liaoning Province (2019-BS-160).

References

Bańka P, Chmiela A, Menéndez Fernández M et al (2017) Predicting changes in induced seismicity on the basis of estimated rock mass energy states. Int J Rock Mech Mining Sci 95:79–86

Baud P, Zhu W, Wong TF (2000) Failure mode and weakening effect of water on sandstone. J Geophys Res Sol Ea 105(B7):16371–16389. https://doi.org/10.1029/2000JB900087

Bieniawski ZT (1967) Mechanism of brittle fracture of rock: part I—theory of the fracture process. Int J Rock Mech Mining Sci 4(4):395–406. https://doi.org/10.1016/0148-9062(67):90030-7

Brace WF, Paulding BR, Scholz C (1966) Dilatancy in fracture of crystalline rocks. Geophys Res 71(16):3939–3953. https://doi.org/10.1029/JZ071i016p03939

Bruno MS, Nakagawa FM (1991) Pore pressure influence on tensile fracture propagation in sedimentary rock. Int J Rock Mech Min Sci Geomech Abstr 28(4):261–327. https://doi.org/10.1016/0148-9062(91)90593-B

Cai MF, Wang JA, Wang SH (2001) Analysis on energy distribution and prediction of rock burst during deep mining excavation in Linglong Gold Mine. Chin J Rock Mech Eng 20(1):38–42

Chen GQ, Wu JC, Jiang WZ, Li SJ, Qiao ZB, Yang WB (2020) An evaluation method of rock brittleness based on the whole process of elastic energy evolution. Chin J Rock Mech Eng 39(5):901–911

Cho JW, Kim H, Jeon S, Min KB (2012) Deformation and strength anisotropy of Asan gneiss, Boryeong shale, and Yeoncheon schist. Int J Rock Mech Mining Sci 50:158–169

Detournay E, Cheng HD, Roegiers JC, Mclennan JD (1989) Poroelasticity considerations in In Situ stress determination by hydraulic fracturing. Int J Rock Mech Min Sci Geomech Abstr 26(6):507–513. https://doi.org/10.1016/0148-9062(89)91428-9

Diederichs MS, Kaiser PK, Eberhardt E (2004) Damage initiation and propagation in hard rock during tunnelling and the influence of near-face stress rotation. Int J Rock Mech Mining Sci 41(5):785–812. https://doi.org/10.1016/j.ijrmms.2004.02.003

Donath FA (1964) Strength variation and deformational behavior in anisotropic rock. In: Judd WR (ed) State of stress in the Earth's crust. Elsevier, New York, pp 281–297

Eberhardt E, Stead D, Stimpson B, Read RS (1998) Identifying crack initiation and propagation thresholds in brittle rock. Can Geotech J 35(2):222–233. https://doi.org/10.1139/t97-091

Eeckhout EMV (1976) The mechanisms of strength reduction due to moisture in coal mine shales. Int J Rock Mech Min Sci Geomech Abstr 13(2):61–67. https://doi.org/10.1016/0148-9062(76)90705-1

GB/T 50266-2013 (2013) Standard for testsmethod of engineering rock masses. China Planning Press, Beijing

Gholami R, Rasouli V (2014) Mechanical and elastic properties of transversely isotropic slate. Rock Mech Rock Eng 47(5):1763–1773. https://doi.org/10.1007/s00603-013-0488-2

Goodman RE (1989) Introduction to rock mechanics, 2nd edn. Wiley, New York

Griffith AA (1921) The phenomena of rupture and flow in solids. Philosophical Transactions of the Royal Society of London. Series a, Containing Papers of a Mathematical or Physical Character 221:163–198

Guo FL, Zhang DL, Su J, Xiao CM (2007) Experimental study on influences of groundwater and confining pressure on mechanical behaviors of soft rocks. Chin J Rock Mech Eng 26(11):2324–2332

Hallbauer DK, Wagner H, Cook NGW (1973) Some observations concerning the microscopic and mechanical behaviour of quartzite specimens in stiff, triaxial compression tests. Int J Rock Mech Min Sci Geomech Abstr 10(6):713–726. https://doi.org/10.1016/0148-9062(73)90015-6

Haberfield CM, Johnston IW (1990) Determination of the fracture toughness of a saturated soft rock. Can Geotech J 27(3):276–284. https://doi.org/10.1139/t90-038

Hoek E (1964) Fracture of anisotropic rock. J S Afr I Min Metall 64(10):501–523

Hudson JA, Brown ET, Fairhurst C (1972) Shape of the complete stress-strain curve for rock. Proceedings of the 13th U.S. Symposium on Rock Mechanics, Urbana

Khanlari G, Rafiei B, Abdilor Y (2015) An experimental investigation of the Brazilian tensile strength and failure patterns of Laminated Sandstones. Rock Mech Rock Eng 48(2):843–852. https://doi.org/10.1007/s00603-014-0576-y

Kidybinski A (1981) Bursting liability indices of coal. Int J Rock Mech Min Sci Geomech Abstr 18(4):295–304
Kim H, Cho JW, Song I, Min KB (2012) Anisotropy of elastic moduli, P-wave velocities, and thermal conductivities of Asan Gneiss, Boryeong Shale, and Yeoncheon Schist in Korea. Eng Geol 147–148(5):68–77. https://doi.org/10.1016/j.enggeo.2012.07.015
Liang C, Wu S, Li X, Xin P (2015) Effects of strain rate on fracture characteristics and mesoscopic failure mechanisms of granite. Int J Rock Mech Mining Sci 76:146–154
Liu GH, Zhang SG, You ZD et al (1992) Main metamorphic rock groups and metamorphic evolution in Qinling orogenic belt. Geological Publishing House, Beijing
Martin CD (1997) The effect of cohesion loss and stress path on brittle rock strength. Can Geotech J 34(5):698–725. https://doi.org/10.1139/t97-030
Martin CD, Chandler NA (1994) The progressive fracture of Lac du Bonnet granite. Int J Rock Mech Min Sci Geomech Abstr 31(6):643–659. https://doi.org/10.1016/0148-9062(94)90005-1
Mclamore R, Gray KE (1967) The mechanical behavior of anisotropic sedimentary rocks. J Eng Ind 89(1):62–73. https://doi.org/10.1115/1.3610013
Mikhalyuk AV, Zakharov VV (1997) Dissipation of dynamic-loading energy in quasi-elastic deformation processes in rocks. J Appl Mech Tech Phys 38(2):312–318. https://doi.org/10.1007/BF02467918
Nasseri MH, Rao K, Ramamurthy T (2003) Transversely isotropic strength and deformational behavior of Himalayan schists. Int J Rock Mech Min Sci 40:3–23. https://doi.org/10.1016/S1365-1609(02)00103-X
Park CH, Bobet A (2010) Crack initiation, propagation and coalescence from frictional flaws in uniaxial compression. Eng Fract Mech 77(14):2727–2748. https://doi.org/10.1016/j.engfracmech.2010.06.027
Peng S, Johnson AM (1970) Crack growth and faulting in cylindrical specimens of Chelmsford Granite. Int J Rock Mech Mining Sci 9(1):37–86. https://doi.org/10.1016/0148-9062(72)90050-2
Ramamurthy T (1993) Strength, modulus responses of anisotropic rocks. In: Hudson JA (ed) Compressive rock engineering, vol 1. Pergamon, Oxford, pp 313–329
Rawling GC, Baud P, Tengfong W (2002) Dilatancy, brittle strength, and anisotropy of foliated rocks: experimental deformation and micromechanical modeling. J Geophys Res 107(B10):2234–2247. https://doi.org/10.1029/2001JB000472
Rossi P (1991) A physical phenomenon which can explain the mechanical behaviour of concrete under high strain rates. Mater Struct 24(6):422–424
Roy DG, Singh TN, Kodikara J, Das R (2017) Effect of water saturation on the fracture and mechanical properties of sedimentary rocks. Rock Mech Rock Eng 50(10):1–16. https://doi.org/10.1007/s00603-017-1253-8
Singh J, Ramamurthy T, Rao GV (1989) Strength anisotropies in rocks. Ind Geotech J 19(2):147–166
Steffler ED, Epstein JS, Conley EG (2003) Energy partitioning for a crack under remote shear and compression. Int J Fracture 120:563–580. https://doi.org/10.1023/A:1025511703698
Sujatha V, Kishen C (2003) Energy release rate due to friction at bi-material interface in dams. J Eng Mech 129(7):793–800
Vishal V, Ranjith PG, Singh TN (2015) An experimental investigation on behaviour of coal under fluid saturation, using acoustic emission. J Nat Gas Sci Eng 22:428–436. https://doi.org/10.1016/j.jngse.2014.12.020
Wang H, Jin W, Li Q (2009) Saturation effect on dynamic tensile and compressive strength of concrete. Adv Struct Eng 12(2):279–286. https://doi.org/10.1260/136943309788251713
Xia D, Yang TH, Xu T, Wang PT, Zhao YC (2015) Experimental study on AE properties during the damage process of water-saturated rock specimens based on time effect. J China Coal Soc 40(S2):337–345
Xie HP, Ju Y, Li LY (2005) Criteria for strength and structural failure of rocks based on energy dissipation and energy release principles. Chin J Rock Mech Eng 24(17):3003–3010
Yang JM, Qiao L, Li Y, Li QW, Li M (2019) Effect of bedding dip on energy evolution and rockburst tendency of loaded phyllite. Chin J Eng 41(10):1258–1265
Yao Q, Chen T, Ju M, Liang S, Liu Y, Li X (2016) Effects of water intrusion on mechanical properties of and crack propagation in coal. Rock Mech Rock Eng 49(12):1–11. https://doi.org/10.1007/s00603-016-1079-9
Yin XM, Yan EC, Wang LN, Liu LC, Feng B, Wang PZ (2020) Anisotropy of quartz mica schist based on quantitative extraction of fabric information. B Eng Geol Environ 79(5):2439–2456. https://doi.org/10.1007/s10064-019-01699-5
Zhang QB, Zhao J (2013) Effect of loading rate on fracture toughness and failure micromechanisms in marble. Eng Fract Mech 102(2):288–309. https://doi.org/10.1016/j.engfracmech.2013.02.009
Zhang J, Ai C, Li YW, Zeng J, Qiu DZ (2017) Brittleness evaluation index based on energy variation in the whole process of rock failure. Chin J Rock Mech Eng 36(6):1326–1340
Zhao Z, Yang J, Zhang D, Peng H (2016) Effects of wetting and cyclic wetting–drying on tensile strength of sandstone with a low clay mineral content. Rock Mech Rock Eng 50(2):1–7. https://doi.org/10.1007/s00603-016-1087-9
Zhou CY, Deng YM, Tan XS, Liu ZQ, Lin CX (2003) Research on the variation regularities of microstructures. Acta Sci Natur Univ Sunyatseni 42(4):98–102
Zhou CY, Tan XS, Deng YM, Zhang YM, Wang JH (2005) Research on softening micro-mechanism of special soft rocks. Chin J Rock Mech Eng 24(3):394–400
Zhou GZ, Liou JG, Liu YJ et al (1996) High and ultrahigh pressure metamorphic belts in Northern Hubei. China University of Geosciences Press, Wuhan